CHAPTER V

n-OCTANE AROMATIZATION OVER Pt/KL OF VARYING MORPHOLOGY AND CHANNEL LENGTHS*

5.1 Abstract

Various Pt/KL catalysts were prepared over a series of zeolites with different crystallite sizes and shapes. To control the crystallite size and shape and consequently the channel lengths, different zeolite synthesis parameters were varied. X-ray diffraction (XRD) analysis of the synthesized KL zeolites indicated a high degree of crystallinity in all samples. The crystallite morphologies and the length/diameter (L/D) ratios in each sample were characterized by scanning electron microscopy (SEM). The Pt/KL catalysts were prepared by loading 1 wt% of Pt on these supports, using the vapor phase impregnation (VPI) method. They were characterized by diffuse reflectance infrared fourier transform spectroscopy (DRIFTS) of adsorbed CO, volumetric hydrogen chemisorption, and transmission electron microscopy (TEM).

It was found that KL zeolites with cylindrical shape are effective catalyst supports for n-octane aromatization, but the effectiveness strongly depends on the channel length of the zeolite crystallite as well as Pt dispersion and location of the Pt cluster. The different Pt/KL catalysts in the series were compared in the aromatization of n-octane at 500°C and atmospheric pressure. It was found that the catalysts with shorter channel length exhibited improved activity, selectivity, and catalyst life.

Some of these differences can be ascribed to a different distribution of Pt clusters and different metal dispersions. That is, while the cylindrical-shape KL zeolites with short channels (i.e. cylindrical crystallites with low L/D ratio) favored a high dispersion of Pt inside the zeolite, those with longer channels (i.e. high L/D ratio) resulted in a large fraction of Pt cluster outside the zeolite. In contrast, KL

---

* Published in Applied Catalysis A: General (2006), 313, 189-199.

zeolites synthesized with nanosize crystallites and having a high external-to-internal surface area ratio yield much lower Pt dispersions and exhibited a large fraction of Pt clusters located outside the pores, which can explain the differences in activity and selectivity. On the other hand, differences in aromatic product distribution observed for the different morphologies are related to a varying extent of secondary reactions. That is, for a given conversion level, the catalysts with shorter channels had a much lower extent of secondary hydrogenolysis. Consequently, more C8 aromatics are preserved in the product and less benzene and toluene are produced compared to the catalysts with longer channels.

5.2 Introduction

The aromatization of *n*-alkanes is an important industrial process to obtain high value-added aromatic products from low-value naphtha streams that may be abundant in a refinery. This reaction has been commercially implemented using either bifunctional (acid-metal) or monofunctional (only-metal) catalysts. One of the advantages of the monofunctional catalysts is the elimination of the isomerization paths that typically occur with the bifunctional catalysts, resulting in a lower selectivity to aromatics [1]. Platinum clusters in alkaline LTL zeolite are very efficient for the direct dehydrocyclization of *n*-hexane into benzene [2-5]. However, they have not been as effective when the feed is *n*-octane [6]. Although Pt/KL catalysts prepared by vapor phase impregnation (VPI) result in very high Pt dispersion and maximum incorporation of Pt inside the channels of the zeolite [7,8], the activity for *n*-octane aromatization is much lower than that of n-hexane and rapidly drops, compared to the almost total absence of deactivation with the n-hexane feed. The product distribution obtained from the *n*-octane conversion yielded benzene and toluene as the dominant aromatic compounds, with small quantities of ethylbenzene (EB) and o-xylene (OX), which are the expected products of a direct six membered ring closure. Since the pore size of the KL zeolite is 0.71 nm [9], larger than the critical diameter of EB but smaller than that of OX, OX diffuses much slower than EB. As a result, OX would preferentially convert to benzene and toluene before escaping from the pore of zeolite. It was also proposed that the pore length of

the zeolite has a great impact on product distribution and catalyst life. However, Pt/KL catalysts exhibited the best performance for n-octane aromatization among other large pore zeolites because the structure of KL zeolite can stabilize high dispersion of Pt clusters inside the pore [10].

It is therefore a reasonable assumption that the catalytic performance of a Pt/KL zeolite may greatly vary with crystallite morphology. For example, it is known [11] that relatively low extents of Pt agglomeration and coking may cause Pt entombment when the zeolite contains one-dimensional long channels. Therefore, Treacy et al. (1999) [12] have proposed that by using KL zeolites with short channels one can minimize the problem of Pt entombment. Other advantages of short-channel zeolites would include enhanced external surface area to mass ratio, which should result in enhanced diffusion rates and reactivities [13]. Fortunately, there is ample evidence in the literature that by adjusting the gel composition it is possible to obtain different crystallite morphologies, e.g., spherical, cylindrical, clam shaped, and disc shaped [14-20]. One of the strategies used to produce short channels has been to synthesize the zeolite with flat basal planes and reduced crystallize size [21-23]. With this aim in mind, researchers have found that the addition of small amounts of divalent cations such as magnesium or barium enhances the formation of flat basal planes. The presence of these ions results in small crystals with low L/D ratios. An added benefit to the presence of Mg or Ba ions is the inhibition to the formation of crystalline contaminants, such as zeolite W and erionite. Exxon researchers have observed that Pt/KL zeolites with very flat cylinder shape (coin or hockeypuck shape) gave greater selectivity and yield as well as allowed for a greatly increased cycle length in comparison with Pt/KL catalysts prepared over a typical clam-shaped KL zeolite [22].

In this study, we have investigated the effects of varying morphology and channel length of the KL zeolite on the n-octane aromatization reaction. As mentioned above, this is a much more demanding reaction than the more widely investigated n-hexane aromatization [6]. In the first step, KL zeolites with varying morphology and channel length were synthesized using the conventional-hydrothermal treatment and microwave-hydrothermal treatment. The synthesized KL zeolites were characterized by XRD, nitrogen adsorption, and SEM.

Subsequently, Pt was incorporated in the various zeolites by the VPI method described in our previous studies [6]. The fresh catalysts were characterized by the FTIR of adsorbed CO. As previously shown [6-8,24,25], this technique can be used to predict the location of the Pt particles in the KL zeolites. Furthermore, hydrogen chemisorption and TEM analysis were performed on the fresh catalysts to estimate the metal dispersion. The activity and selectivity of all the catalysts in the series for the *n*-octane aromatization were compared at 500°C and atmospheric pressure. The amount of coke deposited on the spent catalysts during reaction was determined by temperature programmed oxidation (TPO).

5.3 Experimental

5.3.1 Synthesis of KL Zeolites and Preparation of Pt/KL Catalysts

Following the procedures described in the Exxon patents [15,18,22], four different KL zeolite morphologies were synthesized: coin-shaped or hockeypuck (HOP), cylinder (CYL), long cylinder (LCYL), and clam-like shape (CLAM). In each case, the potassium aluminate solution was prepared by dissolving $Al(OH)_3$ in KOH solution. The preparation of the silicate solution depended on the desired morphology. For the HOP sample, this solution was prepared by mixing colloidal silica with $Ba(OH)_2$ solution and stirring for 15 min. For the other three morphologies (CYL, LCYL and CLAM), no barium was added. The silicate and aluminate solutions were then mixed and stirred vigorously to obtain a homogeneous gel mixture at ambient temperature. The resulting gel mixture was transferred into a Teflon-lined 250 ml autoclave for crystallization. The experimental details of gel composition, stirring, and period of crystallization are summarized in Table 5.1

Table 5.1 Gel composition and synthesis conditions

Morpholgies of KL zeolites	Gel composition (mole)					Stirred time (h)	Cryst. time (h)	Temp (°C)
	K_2O	Al_2O_3	SiO_2	H_2O	BaO			
Hockeypuck (HOP)	2.62	0.5	10	160	0.0032	17	96	170
Cylinder (CYL)	2.62	1	10	160	-	17	120	150
Long Cylinder (LCYL)	2.21	1	9	164.4	-	24	96	175
CLAM	3.5	1	10	160	-	24	120	150
Nanocrystal* (NCL)	10	1	20	400	-	17	8	175

*synthesized by microwave-hydrothermal treatment, all the other were synthesized by conventional-hydrothermal treatment

In the synthesis of the nano-crystalline KL zeolite, a gel composition of $10K_2O$: $1Al_2O_3$: $20SiO_2$: $400H_2O$ was introduced following previously published methods [26]. First, the silicate solution was prepared by mixing 54 g of colloidal silica with 60 ml of deionized water and stirring for 15 min. Then, the potassium aluminate solution was prepared by dissolving 2.8 g of $Al(OH)_3$ in the 36 ml of 11.5 M of KOH solution with stirring and heating at 80 °C for 30 min. After that, the silicate and aluminate solutions were then mixed and stirred vigorously by a mechanical stirrer for 17 h at ambient temperature. Next, the gel mixture was transferred to a microwave vessel and heated at the power of 600 W, using a MARS5 microwave machine, up to 175°C within 2 minutes and maintained at that temperature for 8 h to bring about the crystallization. After crystallization, the obtained material was washed with deionized water until reaching pH 10 and then centrifuged to separate the solution from the solid deposit, which was later dried in an oven at 110°C overnight and then calcined at 500°C in flowing air. For a comparison, a commercial KL zeolite (from Tosho company, HSZ-500, SiO_2/Al_2O_3=6) was included in the series. This sample is indicated as COM.

It must be noted that the composition of some of the zeolites employed in this study may not be exactly the same. The reason for this difference is that changes in composition are in some cases needed in order to control the morphology of the KL zeolite. For example, in the case of nanocrystal KL zeolite (NCL), the concentration of K_2O should be increased to increase the density of nuclei and thus reduce the size of KL crystallites. Likewise, for the HOP synthesis, the amount of Al_2O_3 must be decreased in order to reduce the length of the cylindrical KL crystallite. Since the KL zeolite is non-acidic we believe that it does not play a significant chemical role during the aromatization reaction; therefore, we have assumed that the slight differences in composition are minor compared to the major differences in zeolite morphology.

The Pt/KL catalysts were prepared by vapor phase impregnation (VPI) of the zeolites of varying morphologies. Prior to impregnation, the zeolite supports were dried in an oven at 110°C overnight and calcined at 500 °C in flowing dry air at a flow rate of 100 cm^3/min.g for 5 h. The Pt/KL catalysts were prepared by

physically mixing weighed amounts of platinum (II) acetylacetonate (Alfa Aesar) with the dried support under nitrogen atmosphere. The mixture was then loaded in a tube reactor and heated in a helium flow of 5 cm^3/min.g. The reactor was first heated in a linear ramp to 40°C and held for 3 h. In the next step, it was heated in a ramp to 60°C and held for 1 h. Finally, it was further heated to 110°C and held for 1 h to complete the sublimation of $Pt(AcAc)_2$. After cooling down to room temperature, the material was heated in a linear ramp to 350°C in flowing air for 2 h to decompose the platinum precursor. The resulting materials were stored in the oxidic form.

5.3.2 Catalyst Characterization

5.3.2.1 Zeolite Supports

The zeolite structures of the synthesized KL zeolites were characterized in a Rigaku X-Ray diffractometer (Cu Kα, scanning rate of 5°/s). The size and morphology of the zeolite crystals were assessed using a JEOL 5200-2AE scanning electron microscope (SEM). Surface area and pore volume of the synthesized KL zeolites were determined by nitrogen adsorption at 77K employing a Thermo Finnigan sorptomatic, 1100 series.

5.3.2.2 Diffuse Reflectance Infrared Fourier Transform Spectroscopy (DRIFTS) of Adsorbed CO

The series of different Pt/KL catalysts was characterized by DRIFTS of adsorbed CO in a Bruker Equinox 55 spectroscope equipped with an MCT detector. Experiments were performed in a diffuse reflectance cell from Harrick Scientific, type HVC-DR2 equipped with ZnSe windows. For each IR spectrum, a background was collected on the sample reduced in situ under a flow of H_2 at 300°C for 1 h and purged in He for 30 min at ambient temperature. Then, a flow of 5%CO in He was passed through the sample for 30 min, followed by purge in He flow for 30 min. After such a treatment, the spectrum of adsorbed CO was collected.

5.3.2.3 Hydrogen Chemisorption

Hydrogen uptakes were obtained by using a pulse technique (Thermo Finnigan model TPDRO 1100). Prior to the chemisorption measurements,

the samples were reduced in H_2 atmosphere at 500°C for 1 h. Consecutively, they were purged with N_2 at 500°C for 30 min and cooled down to 50°C in flowing N_2. A H_2 pulse (purged H_2, 0.4 ml) was injected onto each sample at 50°C.

5.3.2.4 Transmission Electron Microscopy (TEM)

The TEM images of the catalysts were acquired in a JEOL JEM-2000FX electron microscope. The pre-reduced catalyst samples were ultrasonicated for 5 min in isopropanol until a homogeneous suspension was formed. In each determination, one drop of this mixture was placed over a TEM copper grid and subsequently dried before the analysis.

5.3.2.5 Temperature Programmed Desorption (TPD) of Isopropylamine

Before doing the adsorption of isopropylamine, the 30 mg of sample was heated from RT to 500°C within 2 h and held at that temperature for 1 h under the He flow of 20 ml/min. After that, the sample was cooled to room temperature. Next, the 10 µl of isopropylamine was injected for 3 times for complete adsorption. Then, the 20 ml/min of He was passed through the sample to remove the excess amount of isopropylamine for 3 h. Finally, the sample was heated up to 700°C within 70 min and held for 30 min under the He flow to desorb the adsorbed isopropylamine. The amount of desorbed isopropylamine was analyzed using an MS detector. The MS detector was calibrated using a variable loop volume of 2%propylene balance in He.

5.3.2.6 Temperature Programmed Oxidation (TPO)

This technique was employed to analyze the amount and characteristics of the coke deposited on the catalysts during reaction. TPO of the spent catalysts was performed in a continuous flow of 2%O_2 in He while the temperature was linearly increased with a heating rate of 12°C/min. The oxidation was conducted in a ¼ in. quartz fixed-bed reactor after the spent catalyst had been dried at 110°C overnight, weighted (0.030 g) , and placed between two layers of quartz wool. The sample was further purged at room temperature by flowing 2%O_2 in He for 30 min before the TPO was started. The CO_2 produced by the oxidation of the coke species was converted to methane using a methanizer filled with 15%

Ni/Al_2O_3 and operated at 400°C. The evolution of methane was analyzed using an FID detector.

5.3.4 Catalytic Activity

The catalytic activity studies were conducted at atmospheric pressure in a ½ inch diameter glass tube reactor equipped with an internal K-type thermocouple for temperature measurements. In the continuous-flow reactor, 0.2 g of fresh catalyst was used in each run. Prior to reaction, the catalyst was slowly ramped in flowing H_2 for 2 h up to 500°C and in-situ reduced at that temperature for 1 h. The *n*-octane feed was continuously injected from a syringe pump, keeping in all the experiments a hydrogen to *n*-octane molar ratio of 6:1. The products were analyzed by gas chromatography using a Shimadzu 17A-GC equipped with an HP-PLOT/Al_2O_3 "S" deactivated capillary column. The GC column temperature was programmed to obtain an adequate separation of the products. The temperature was first kept constant at 40°C for 10 min and then, linearly ramped to 195°C and held for 30 min.

5.4 Results and Discussion

5.4.1 KL Zeolites of Varying Morphology and Channel Length

The KL zeolites synthesized following the different procedures were characterized by XRD, SEM, and BET surface area measurement. The XRD patterns of the synthesized KL zeolites were compared to that of the commercial KL zeolite (COM) as shown in Figure 5.1(a). The patterns indicate that all samples were highly crystalline LTL-type material, without any trace of other crystalline phases or amorphous materials. In addition, all synthesized KL zeolites have very similar surface areas and pore volumes to those of the commercial KL zeolite (COM).

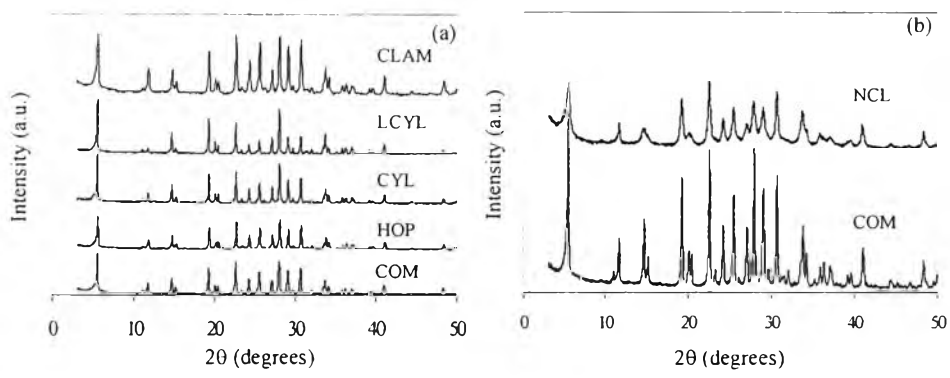

Figure 5.1 XRD patterns of synthesized KL zeolites.

From the SEM measurements, it can be observed that the different synthesis procedures resulted in different morphologies, as anticipated from the previous studies used as reference for the synthesis [14-20]. The SEM images of the hockeypuck (HOP), cylinder (CYL), long cylinder (LCYL), and clam (CLAM) shapes are illustrated in Figure 5.2. It is obvious that these three morphologies exhibit very different aspect ratios (i.e. length to diameter of the cylinder) as summarized in Table 5.2: the HOP (very flat cylinders) has an aspect ratio of around 0.34, while the CYL and LCYL have aspect ratios of around 1.28 and 2.33, respectively. In the case of the clam-shaped crystals an aspect ratio cannot be established since they have rough domed basal planes. However, from the SEM images the crystal size can be estimated around 0.5-0.8 μm.

As shown in Figure 5.1(b) the nano-crystalline KL, synthesized by the microwave-hydrothermal treatment, exhibited very broad XRD peaks, indicative of the presence of very small crystals [27]. In good agreement, the TEM images depicted in Figure 5.3 indicate that indeed the zeolite crystals have dimensions of approximately 15 nm in the channel direction; however, these crystals tend to agglomerate into larger clusters of about 0.20 μm, which is the size determined by the DLS method.

Another way of getting a direct measure of the different morphology of the various zeolites is by means of XRD. The peak intensity ratio between the d(100) for the prismatic face and that of the d(001) for pinacoidal face is expected to

increase with the aspect [20]. As shown in Table 5.2, the values of this ratio correlate well with the aspect ratio as determined by SEM. This ratio allows for a more or less quantitative comparison of the anisotropy of the crystals even for samples like COM, CLAM, and NCL, which do not show enough regularity to obtain an aspect ratio from SEM observations. In all these three cases, the prismatic/pyramidal ratio was very low, indicating a small aspect ratio.

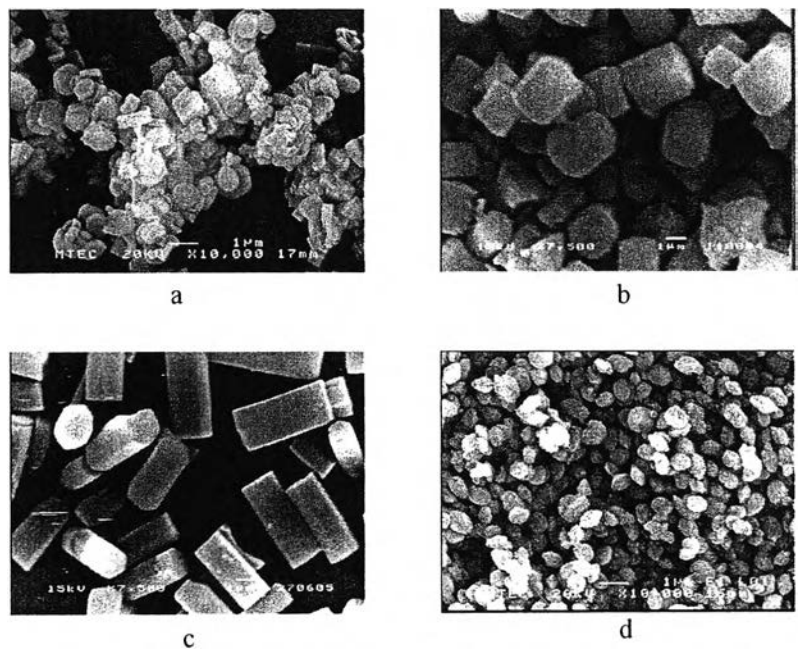

Figure 5.2 SEM images of synthesized KL zeolites (a) HOP (b) CYL (c) LCYL and (d) CLAM.

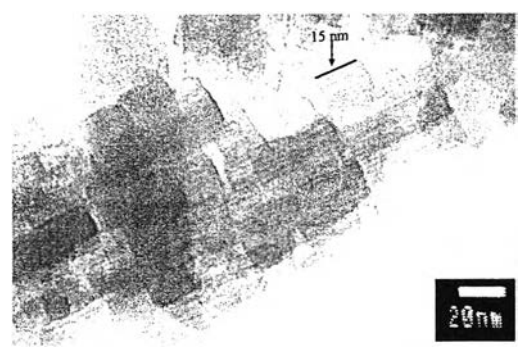

Figure 5.3 TEM image of synthesized L nanocrystal (NCL) using MH at 175°C for 8 h.

Table 5.2 Characterization data of synthesized KL zeolites

KL zeolites	Morphologies	Aspect ratio (L/D)**	XRD prismatic/ pinacoidal	Crystallite size (μm)	Surface area (m^2/g)	Pore volume (cc/g)
COM	n/a	n/a	3.0	0.53*	302	0.206
HOP	Hockeypuck	0.34	2.9	(0.28-0.4)× (0.83-1.10)**	254	0.157
CYL	Cylinder	1.28	4.4	(1.97-2.37)× (2.60-3.03)**	263	0.148
LCYL	Long Cylinder	2.33	9.1	(1.68-2,14)× (3.97-5.00)**	233	0.142
CLAM	Clam	n/a	2.2	0.5-0.8**	306	0.248
NCL	Nanocrystal	n/a	2.0	0.20*	368	0.617

*measured by DLS

**measured by SEM

5.4.2 Distribution of Pt on the KL Zeolites of Varying Morphology and Channel Length

The fresh Pt/KL catalysts prepared by VPI over the different KL zeolites were characterized by TEM analysis, H_2 and CO chemisorptions. As indicated in Table 5.3, the H/Pt ratios obtained for the Pt/KL(HOP) and Pt/CLAM were greater than unity, which is consistent with the formation of Pt clusters smaller than 1 nm in size, as previously observed [28]. In contrast, the H/Pt ratios obtained on Pt/KL(CYL) and Pt/KL(LCYL) were less than unity. It is obvious from these results that one of the major advantages of using short-channel KL zeolites resides in the distribution of the Pt clusters. It is possible that during the thermal pretreatment, the evolution of precursor residues (during calcination) and/or water (during reduction) causes the migration of Pt along the channels with consequent agglomeration outside the zeolite. As a result, the longer the channel the more aggravated is the agglomeration phenomenon.

Table 5.3 Analysis of the fresh and spent catalysts

Catalysts	Support	Aspect ratio (L/D)	Fresh catalysts		Spent catalysts
			Pt (wt%)	H/Pt ratio after reduction at 500°C	Coke deposited after rxn with n-C8 for 550 min (wt%)
1%Pt/HOP	HOP	0.23	1.00	1.31	0.89
1%Pt/CYL	CYL	1.21		0.66	1.46
1%Pt/LCYL	LCYL	2.33		0.70	0.72
1%Pt/CLAM	CLAM	n/a		1.46	2.21
0.6%Pt/NCL	NCL	n/a	0.60	0.80	2.28

To quantify the degree of Pt agglomeration outside the channels of the zeolite we have used FTIR of adsorbed CO, a technique that we have employed in several previous investigations to determine the location of the Pt clusters on KL zeolites [7,8]. As described previously, typical FTIR of CO adsorbed on Pt/KL exhibits bands between 2150 and 1900 cm^{-1}. The bands in the region below 2050 cm^{-1} correspond to Pt clusters located inside the channels of the L zeolite. The band between 2050 cm^{-1} and 2075 cm^{-1} is associated with larger Pt cluster at the pore mouth of the L zeolite while the band above 2075 cm^{-1} reflects the presence of Pt clusters located outside of the zeolite pore. The DRIFTS spectra of the catalysts in the series depicted in Figure 5.4 indicate that all of them have a fraction of Pt located inside the pore; however, the Pt/KL(CYL) and Pt/KL(LCYL) samples exhibited a larger fraction of Pt clusters outside the zeolite pores than that observed on the Pt/KL(HOP) catalyst. Table 5.5 summarizes the results obtained by integrating the band areas for the three regions.

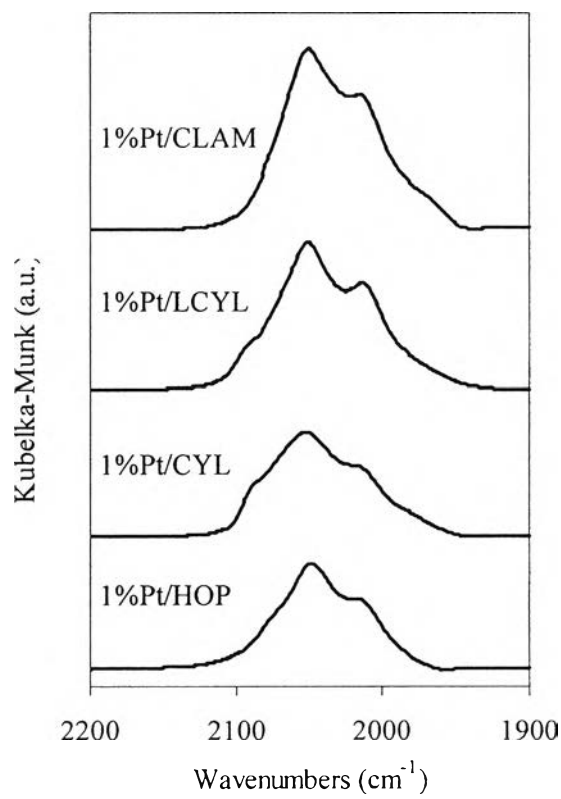

Figure 5.4 DRIFTS spectra of CO adsorbed on different channel lengths of Pt/KL catalysts.

The FTIR results are in good correspondence with the TEM images obtained on the different samples, as shown in Figure 5.5. The zeolites with the longer channels Pt/KL(CYL) and Pt/KL(LCYL) had a larger fraction of Pt clusters outside the pore structure, as well as larger Pt particle sizes. It is very interesting to note that that not only the zeolites with long channel length result in low Pt dispersion. The nano-crystalline KL zeolite also works against a good dispersion of the Pt cluster. As indicated in Table 5.4, the 1%Pt/NCL having the smaller zeolite crystallite size yields the lowest Pt dispersion, comparable to the 1%Pt/COM catalyst, which has a large zeolite crystallite size. It is expected that, when the crystal size of the zeolite is too small, the external surface area dominates [29,30]. Consequently, there is a high possibility that an important fraction of the platinum cluster remains on the external surface, outside the pores. This Pt fraction results in a low H/Pt ratio since the unique ability of the KL pores to stabilize small Pt clusters [6,12,31] is not used. Therefore, there seems to be an intermediate crystallite size for which maximum Pt dispersion can be achieved.

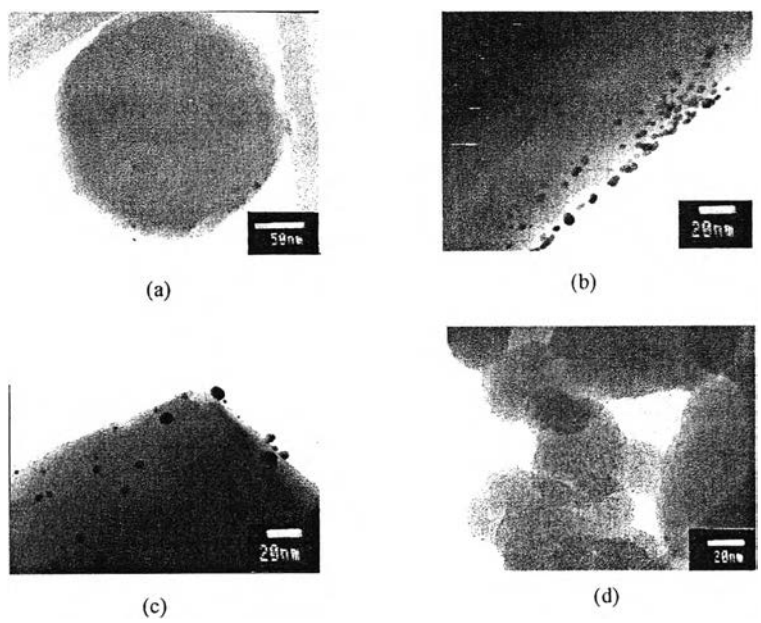

Figure 5.5 TEM images of Pt supported on the different channel lengths of (a) 1%Pt/HOP (b) 1%Pt/CYL (c) 1%Pt/LCYL and (d) 0.6%Pt/NCL after reduction at 500°C for 1 h.

Table 5.4 Effect of the particle size of KL zeolite on Platinum dispersion of Pt/KL catalysts

Catalysts	Support	Particle size (μm)	Fresh Catalysts	
			Pt (wt%)	H/Pt ratio after reduction at 500°C
1%Pt/COM	COM	0.53	0.98	1.48
0.3%Pt/NCL	NCL	0.20	0.36	1.53
0.6%Pt/NCL			0.60	0.80
1%Pt/NCL			0.90	0.45

The TPD of isopropylamine showed no strong acidity in any of these Pt/KL catalysts. After adsorption, small amounts of unreacted isopropylamine were observed to desorb at low temperatures, without undergoing the elimination reaction that only take place on strong Bronsted sites [32]. That is, the masses m/e=17, 41 and 44 ionization fragments of the isopropylamine molecule were all observed simultaneously. By constrast, on acidic zeolites, m/=17 and 41 are typically observed at high temperatures as isopropylamine decomposes. The lack of surface reaction indicateds the absence of strong acidity in all the KL samples investigated.

Table 5.5 Area fraction of Pt location on different channel length KL zeolites

Catalysts	Peak position (cm^{-1})			Conversion after 550 min time on stream (%)
	<2050 (Inside the pore)	2050-2075 (Near the pore mouth)	>2075 (Outside the pore)	
1%Pt/COM	46.80	53.20	0	23.28
1%Pt/HOP	38.50	61.94	0	19.51
1%Pt/CYL	70.83	19.00	10.17	11.25
1%Pt/LCYL	65.90	21.14	12.96	8.91
1%Pt/CLAM	81.70	18.30	0	28.26
0.3%Pt/NCL	70.84	29.19	0	11.80
0.6%Pt/NCL	29.14	70.85	0	16.50
1%Pt/NCL	65.16	19.52	15.32	12.70

5.4.3 Catalytic Activity of the Pt/KL Catalyst Series

5.4.3.1 Effect of Zeolite Channel Length

The crystals with cylindrical shape (CYL, LCYL, HOP) have their channels running parallel to the central axis of the cylinder [26]. Therefore, these zeolites make a perfect set to compare the effect of channel length on activity and selectivity. In addition, NCL with the smallest crystallite size was used to represent the KL zeolite having the shortest channel length. Accordingly, the activity of catalysts with varying channel lengths for the conversion of n-octane is compared in Figure 5.6. Primarily, it was observed that the activity of the Pt/KL catalysts depends on the Pt dispersion as shown in Figure 5.7, that is the activity increases with the Pt dispersion, although there seems to be a range of activity values for a given Pt dispersion. That is not only Pt dispersion but also Pt distribution may influence activity. In fact, the two catalysts that exhibit the lowest conversions are those for which the DRIFTS and TEM analysis indicated that had a significant fraction of Pt particles outside the channels of the zeolite (see Table 5.5). The greater the fraction of Pt outside the channels, the lower is the activity of the catalyst.

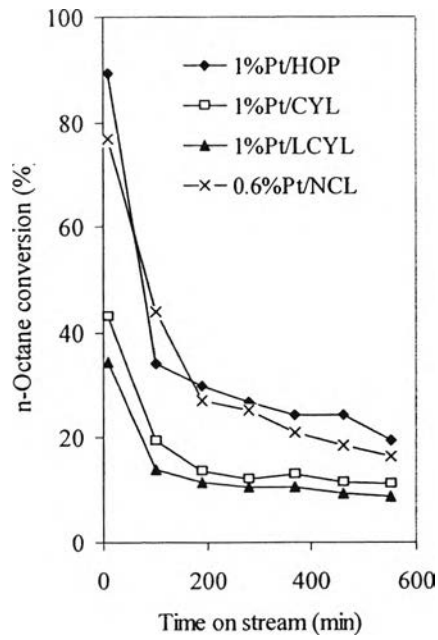

Figure 5.6 The variation of n-octane conversion with time on stream of different channel lengths of Pt/KL catalysts; reaction conditions: temperature = 500°C, pressure = 1 atm, WHSV =5 hr^{-1}, and H_2:HC =6:1.

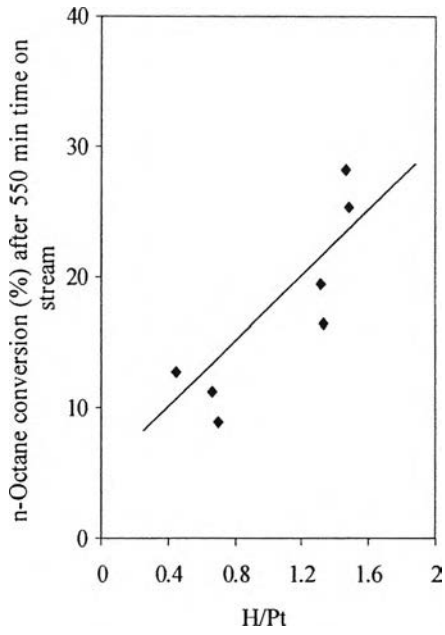

Figure 5.7 The variation of n-octane conversion after 550 min time on stream with Pt dispersion (H/Pt).

At the same time, for the fraction of Pt inside the zeolite channels, the fraction that more greatly enhances the activity is the one inside the pores, like 1%Pt/COM and 1%Pt/CLAM as opposed to those located near the pore mouth. In fact, it has been proposed that the Pt clusters located near the pore mouth and outside the pore mouth are more easily deactivated than those located inside the pores [8]. As summarized in Table 5.5, the conversion remaining after 550 min of time on stream correlates well with the distribution and amount of Pt loading. That is, the conversions for both 1%Pt/COM and 1%Pt/CLAM are very high, consistent with the absence of Pt outside the channels and a high fraction of Pt inside. Conversely, the conversion is lowest for 1%Pt/NCL, 1% Pt/CYL, and 1% Pt/LCY, which have a large fraction of Pt outside the pores. Obviously, although 0.3%Pt/NCL exhibited a high fraction of Pt inside the pores; the observed conversion was less due to the much lower Pt loading.

Regarding selectivity toward aromatics, the 1%Pt/HOP exhibited the highest selectivity to total aromatics, which stayed remarkably high through the whole run, as illustrated in Figure 5.8(a). Although the aromatics products on this HOP catalyst were dominated by benzene and toluene, the

selectivity to C8-aromatics on this catalyst was significantly higher than on those of longer channel lengths, that is CYL and particularly LCYL as shown in Figure 5.8(b). As described above, one can expect that the longer the zeolite channel, the longer is the residence time of the C8 aromatic products inside the zeolite and the higher is the probability of effecting secondary conversion to benzene and smaller molecules.

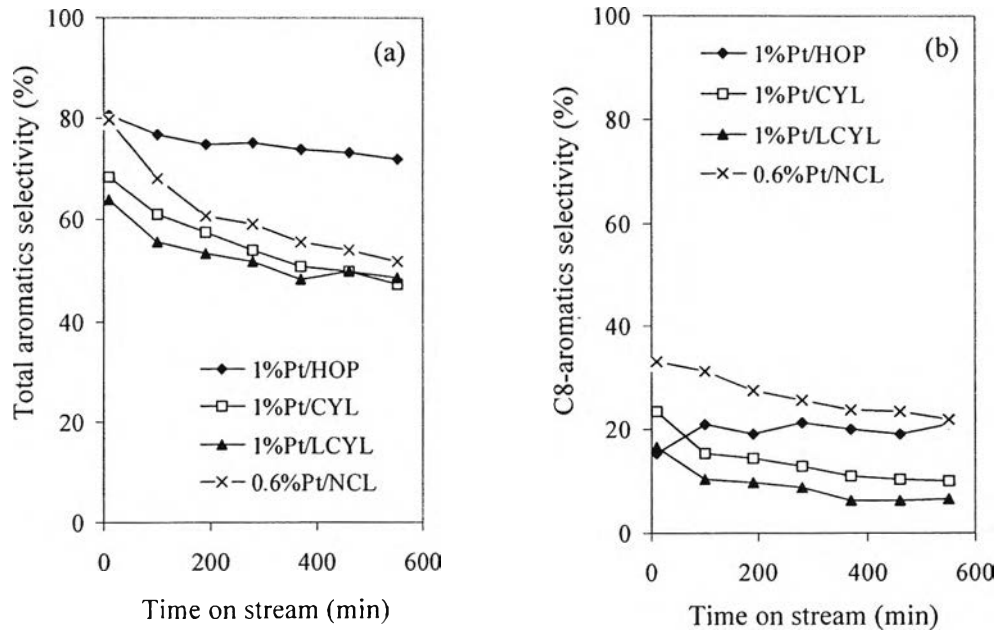

Figure 5.8 The variation of (a) total aromatics selectivity and (b) C8-aromatics selectivity with time on stream of Pt/KL catalysts; reaction conditions: temperature = 500°C, pressure = 1 atm, WHSV =5 h^{-1}, and H_2:HC = 6:1.

The evolution of selectivity to C8-aromatics and benzene as a function of n-octane conversion was shown in Figure 5.9. To vary the overall conversion, runs were conducted at varying contact time (W/F). It is clear that the nano-crystalline KL zeolite (NCL) catalyst results in the highest selectivity to C8-aromatic products as one could have anticipated due to shorter length and therefore lower chance for secondary cracking reactions. It can be concluded that the channel length of KL zeolite plays an important role in determining the aromatic selectivity in the n-octane aromatization reaction. In contrast, no evidence of a correlation between zeolite crystal length and conversion or selectivity was observed with n-

hexane feed [29]. Certainly, with heavier feeds, the molecular transport and secondary reaction effects are much more important [6,10].

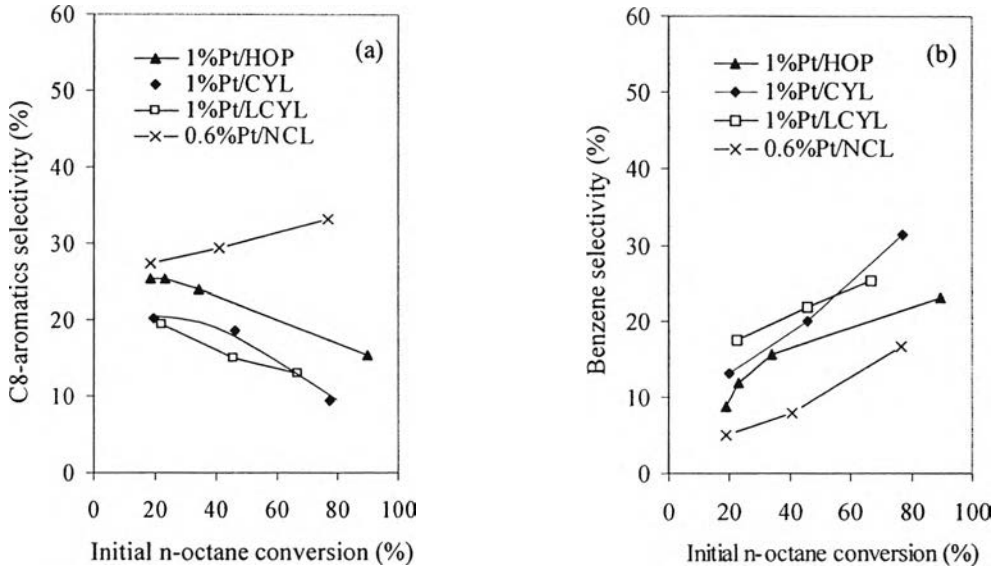

Figure 5.9 The variation of (a) C8-aromatics selectivity (b) benzene selectivity with initial n-octane conversion which is varied by changing the WHSV from 15 to 1 $h^{-1}$of the various Pt/KL catalysts; reaction conditions: temperature = 500°C, pressure = 1 atm, and H_2:HC = 6:1.

As we have identified in previous studies, [6] the analysis of the C8 aromatics distribution can be a good indicator of shape selectivity. For example, ethylbenzene (EB) and orthoxylene (OX) product ratio are primary products produced in about the same ratio. In fact, a product ratio of about unity is observed over Pt/SiO_2 and other nonmicroporous catalysts [6]. On the other hand, the EB/OX ratio becomes greater than 1 when there is pore restriction and it gets greater as the diffusional effects become more pronounced, for example by carbon deposition. Since the critical size of the OX molecule is larger than that of EB, then the speed of transport through the pores is slower for OX than for EB; therefore, OX is more easily converted to smaller molecules such as benzene, toluene, and methane by secondary hydrogenolysis than EB. As shown in Table 5.6, OX is completely converted on the Pt/LCYL catalyst, while significant amounts of OX remain in the

product for the zeolite of smaller crystallite size Pt/NCL. Therefore, it is clear that the selectivity is affected by the channel length.

Nevertheless, it is possible that the channel length may in turn affect the distribution of Pt inside the channel and the location of Pt clusters may have an effect on selectivity. Ideally, if the distribution of Pt in channels of different channel length were similar, the Pt/KL catalyst having the shorter channel length would exhibit a high selectivity to C8-aromatics and less hydrogenolysis products than a catalyst with the longer channels. However, the Pt distribution may not necessarily remain unchanged for different channel lengths. To test these effects, we have conducted an experiment to compare the product selectivity at short contact times and the same overall conversion (60%) as a function of the L/D ratio and the Pt location in several different catalysts. The results clearly show that both effects may be important, but the L/D ratio seems to be more significant. As shown in Figure 5.10(a) and (b), the Pt/KL catalysts with lower L/D ratio and high fraction of Pt located near the pore mouth (i.e., 0.6wt%Pt/NCL and 1wt%Pt/HOP) yielded high selectivity to C8-aromatics products. That is, if the active site is located near the pore mouth, the secondary reaction decreases. (see Table 5.7). However, by comparing Figure 5.10(a) and (b) we can see that for a given distribution of Pt (i.e., the same ratio of Pt near pore moth/Pt inside the pore) the selectivity still varies with the L/D ratio.

Table 5.6 Properties of various catalysts tested for n-octane aromatization after 550 min ; reaction condition: temperature = 500°C, pressure = 1 atm, WHSV = 5 h^{-1}, and H_2:HC = 6:1

Properties	1%Pt/COM	1%Pt/HOP	1%Pt/CYL	1%Pt/LCYL	1%Pt/CLAM	0.6%Pt/NCL
Conversion (%)	23.28	19.51	11.25	8.91	28.26	16.51
Product distribution (%)						
C1-C5	19.72	16.81	34.82	34.18	24.28	20.20
Total enes (C6-C8enes)	12.40	11.12	17.84	17.42	10.11	28.08
Total aromatics	67.88	72.70	47.34	48.40	65.61	51.72
Total aromatics (%)						
Benzene	19.05	17.47	16.87	21.11	20.77	8.17
Toluene	27.59	33.67	20.54	20.72	29.12	21.56
EB	13.95	16.26	7.80	6.57	10.74	14.03
m-.p-Xylene	1.82	0.00	0.00	0.00	1.37	0.00
o-Xylene	5.47	4.67	2.14	0.00	3.61	7.97
Hydrogenolysis Products	66.36	67.95	72.22	76.01	74.17	49.92
EB/OX ratio	2.55	3.48	3.65	-	2.97	1.76
Aspect ratio from XRD	3.00	2.90	4.44	9.10	2.20	2.00

Table 5.7 The influence of the Pt location on the selectivity to hydrogenolysis products at 60% of n-octane conversion

Catalysts	%Pt near pore mouth	$(C_6H_6+C_7H_8)$/Total aromatics*
1%Pt/CLAM	18.30	0.80
1%Pt/CYL	19.00	0.76
1%Pt/LCYL	21.14	0.77
1%Pt/HOP	61.90	0.68
0.6%Pt/NCL	70.85	0.60

*The data were obtained at the initial n-octane conversion of 60%

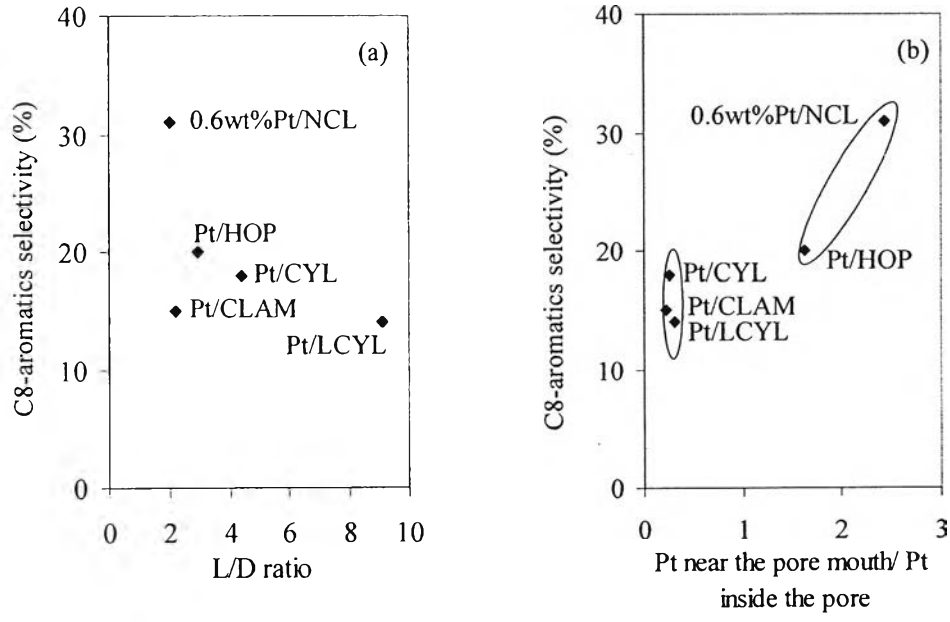

Figure 5.10 The variation of C8-aromatics selectivity at 60% of n-octane conversion with (a) L/ D ratio of HOP, CYL, LCYL, NCL which are calculated from ratio of prismatic to pinacoidal and (b) the ratio of Pt near the pore mouth to Pt inside the pore mouth.

5.4.3.2 Effect of the Zeolite Morphologies

Two Pt/KL catalysts prepared on zeolites with clam (CLAM) and hockeypuck (HOP) shapes were chosen to study the effect of zeolite morphology

on the aromatization of n-octane. This is an interesting comparison since the metal dispersion on these two catalysts is similarly high. The evolution of n-octane conversion for the two catalysts is shown in Figure 5.11 as a function of time on stream. It is clear that the 1% Pt/CLAM exhibits significantly higher activity than 1% Pt/HOP. This enhanced activity can be mostly due to the slightly higher Pt dispersion of the former. However, although these two catalysts had the highest Pt dispersion in the series both of them exhibited a significant deactivation during the first few hours, which as previously shown [6] can be ascribed to pore plugging by coke. It must be noted, that the deactivation model described by McVicker et al. [11] concerning the pore plugging by sintered metal particles is not relevant during the relatively short times of these experiments in the absence of sulfur. The predominant role of coke is demonstrated by the fact that, when using an n-hexane feed, the degree of deactivation is almost insignificant.

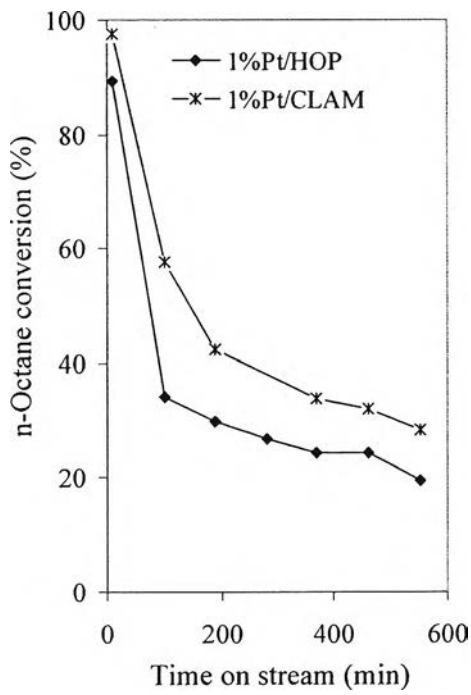

Figure 5.11 The variation of n-octane conversion with time on stream of different morphologies of Pt/KL catalysts; reaction conditions: temperature = 500°C, pressure = 1 atm, WHSV = 5 h^{-1}, and H_2:HC = 6:1.

The total aromatics and C8-aromatics selectivity trends are shown in Figure 5.12 (a) and 5.12(b), respectively. In contrast to the specific activity, the aromatics selectivity is significantly higher for the Pt/HOP than for the Pt/CLAM. This is a rather unexpected result since in most of the previous studies on n-hexane aromatization on Pt/KL catalysts, the most active samples were at the same time the most selective ones. That is, for n-hexane aromatization, activity trends typically parallel selectivity trends [8]. A convenient way of comparing the effectiveness of aromatization catalysts is to plot selectivity as a function of conversion [28]. In the case of n-hexane aromatization, a selective catalyst exhibits benzene selectivities approaching 100% as the conversion increases. By contrast, in the case of n-octane the C8 aromatics selectivity reaches a maximum at relatively low conversions as the C8 aromatics are further converted into benzene and toluene.

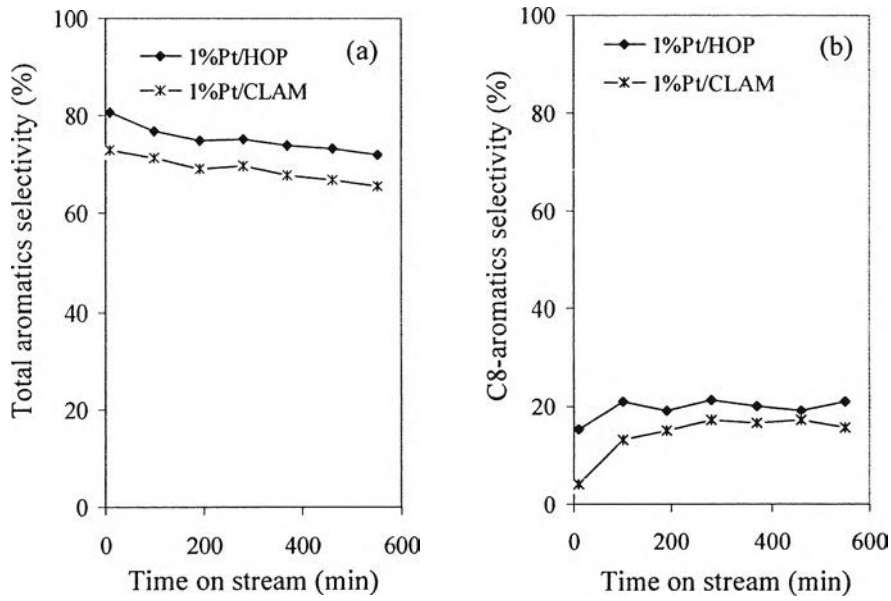

Figure 5.12 The variation of (a) total aromatics selectivity and (b) C8-aromatics selectivity with time on stream of Pt/KL catalysts; reaction conditions: temperature = 500°C, pressure = 1 atm, WHSV = 5 h^{-1}, and H_2:HC = 6:1.

As shown in Figure 5.13(a) and 5.13(b), the morphology of the KL zeolite has a strong influence in the aromatics product distribution. Compared to 1%Pt/HOP, the 1%Pt/CLAM exhibited significantly lower selectivity

to C8-aromatics but higher selectivity to benzene, which is the secondary product arising from hydrogenolysis of the primary products. The higher degree of secondary hydrogenolysis on the CLAM catalyst could be explained in terms of a more restricted circulation for the products out of the zeolite. It has been proposed that the performance of materials with mono- or bi- dimensional pore systems can be strongly affected by the morphology of the zeolite crystals [20]. It is conceivable that because of the jagged terminations, the CLAM zeolite have a higher density of defects at the pore openings causing a more restricted path compared to the smooth terminations of the HOP crystals. As a result, the C8-aromatics would have longer residence times inside the pores, favoring the secondary conversion to smaller aromatics. Furthermore, as summarized in Table 5.3, over the 550 min reaction period, the CLAM catalyst formed significantly higher amounts of coke than the corresponding HOP. This conclusion corresponds well with previous work [15] that reports that the catalyst based on the cylindrical-shaped KL zeolite shows a remarkably improved life for the n-alkane aromatization over extended periods of time, much greater than that achieved with catalysts based on the clam-shaped zeolite L.

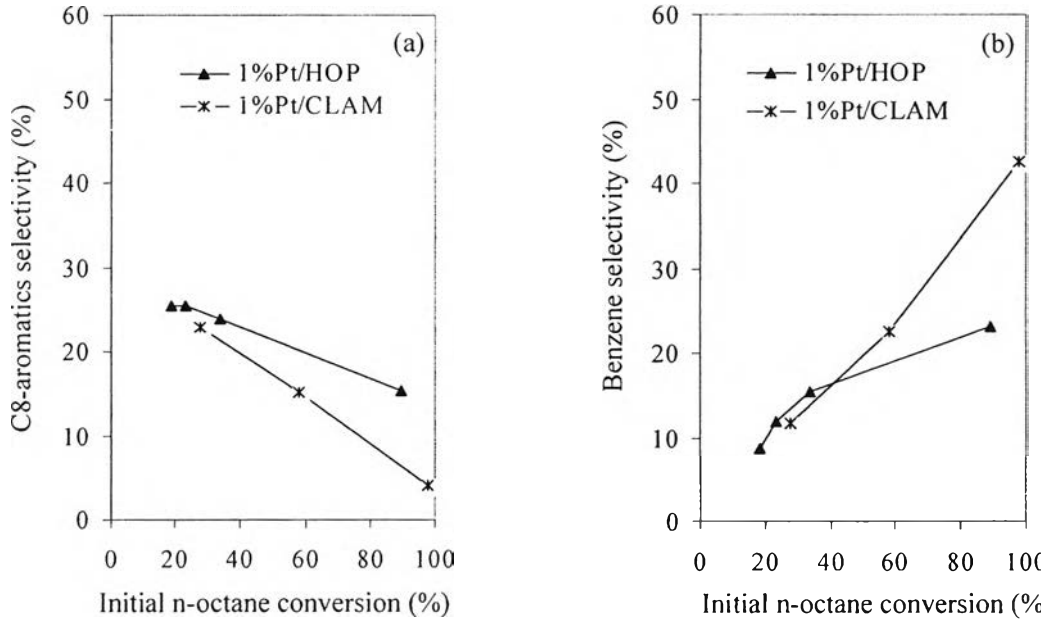

Figure 5.13 The variation of (a) C8-aromatics selectivity (b) benzene selectivity with initial n-octane conversion which is varied by changing the WHSV from 9 to 1 h^{-1} for the various Pt/KL catalysts; reaction conditions: temperature = 500°C, pressure = 1 atm, and H_2:HC = 6:1.

5.4.4 Effects of Varying Morphology and Channel Length on Coke Formation

The spent catalysts were analyzed by temperature programmed oxidation (TPO) to determine the amounts of coke formed after a 550-min time on stream. The results are summarized in Table 5.3. In contrast with the behavior typically observed with n-hexane feeds, the amounts of coke deposited during the n-octane reaction showed no correlation with either Pt dispersion or catalytic activity (final or initial). In fact, the catalyst with the highest final activity accumulated the greatest amount of coke (CLAM). Rather, there seems to be a correlation with the zeolite morphology because no acidity was observed on these series Pt/KL catalysts after the catalysts were characterized by TPD of isopropylamine. That is, the zeolites that exhibited the highest amounts of coke were those with more defective outer surfaces (NCL and CLAM). On the other hand, if one concentrates on the catalysts with smoother crystal terminations (HOP, CYL, and LCYL) one can evaluated the effect of channel length on coke formation. Accordingly, the amount of coke

deposits increases with channel length when one compares HOP with CYL, but it decreases again for the longest crystals (LCYL). One can rationalize this behavior considering that the zeolite with the longest channels may get deactivated with a relatively small amount of coke that would accumulate near the pore mouth.

5.5 Conclusions

The morphology and the channel length of KL zeolites have important effects on the performance of Pt/KL catalysts used for the aromatization of n-octane. The effects can be interpreted in terms of the following aspects:

a) The distribution of aromatic products (ethylbenzene, orthoxylene, toluene, and benzene) is greatly affected by secondary hydrogenolysis reactions. In this regard, zeolites with longer channels and with irregular pore mouth structure prolong the residence time of C8 aromatics and increase the concentration of benzene and toluene in the products. As a result, catalysts with very small crystal size (e.g. NCL) are preferred for producing higher C8 aromatics. In addition, the high selectivity to C8-aromatics can be obtained from the Pt/KL zeolite having more Pt located near the pore mouth.

b) The metal dispersion and distribution of metal clusters inside and outside of the zeolite channels are greatly affected by the zeolite morphology. In turn, the location of metal clusters and Pt dispersion has an important effect on the activity and stability of the catalyst. That is, the catalytic activity increases with Pt dispersion. Furthermore, catalysts with a larger fraction of small metal clusters inside the pores are more active for a longer time. The metal distribution in the zeolite is optimum with intermediate zeolite crystal size. When the crystal is too long, Pt particles can be transported outside of the zeolite during the pretreatments (i.e. reduction). By contrast, when the crystal is too small, the outer surface area dominates and a large fraction of metal particles can be deposited outside the pores.

5.6 Acknowledgements

This work was supported by the Thailand Research Fund (TRF), the Petroleum and Petrochemical Technology Consortium (PPT) through CU-PPC of the Petroleum and Petrochemical College, Chulalongkorn University, and Ratchadapiseksomphot Endowment of Chulalongkorn University, We gratefully acknowledge the Oklahoma Center for Advancement of Science and Technology (OCAST) for providing financial support of the work accomplished at the University of Oklahoma.

5.7 References

1. P. Meriaudeau, C. Naccache, Catal.Rev.Sci.Eng. 39 (1&2) (1997) 5.
2. J.R. Bernard, in; L.V.C. Ress (Ed.), Proceeding in Fifth International Conference on Zeolite, Heyden, London, (1980), p. 686.
3. G. Lane, F.S. Modica, J.T. Miller, J. Catal. 129 (1991) 145.
4. T.R. Hughes, W.C. Buss, P.W. Tamm, R.L. Jacobson, Stud. Surf. Sci. Catal. 28 (1986) 725.
5. P.W. Tamm, D.H. Mohr, C.R. Wilson, Stud. Surf. Sci. Catal. 38 (1988) 335.
6. S. Jongpatiwut, P.Sackamduang, S. Osuwan, T. Rirksomboon, D.E. Resasco, J. Catal. 218 (2003) 1.
7. G. Jacobs, F. Ghadiali, A. Pisano, A. Borgna, W.E. Alvarez, D.E. Resasco, Appl. Catal. 188 (1999) 79.
8. G. Jacobs, W.E. Alvarez, D.E. Resasco, Appl. Catal. A Gen. 206 (2001) 267.
9. J. Arika, S. Italbashi, Y. Tamura, US Pat. 4,530,824 (1985).
10. S. Jongpatiwut, S. Trakarnroek, T. Rirksomboon, S. Osuwan, D.E. Resasco, Catal. Lett. 100 (2005) 7.
11. G.B. Mcvicker, J.L. Kao, J.J. Ziemak, W.E. Gates, J.L. Robbins, M.M.J. Treacy, S.B. Rice, T.H. Vanderspurt, V.R. Cross, A.K. Ghosh, J. Catal. 139 (1993) 48.
12. M.M.J. Treacy, Micropor. Mesopor. Mater. 28 (1999) 271.
13. J.P. Verduijn, M.M. Mertens, M.H. Antanis, US Pat. 6,258,991 B1 (1991).

14. D.W. Breck, N.A. Acara, US Pat. 3,216,789 (1965).
15. T.M. Wortel, US Pat. 4,544,539 (1985).
16. Y.S. Ko, W.S. Ahn, Bull. Korean Chem. Soc. 20 (1999) 1.
17. Y.S. Ko, W.S. Ahn, Powder Technol. 145 (2004) 10.
18. A.Z. Ruiz, D. Bruhwiler, T. Ban, G. Calzaferri, Monatsh. Chem. 136 (2005) 77.
19. Y.J. Lee, J.S. Lee, K.B. Yoon, Micropor. Mesopor. Mater. 80 (2005) 237.
20. O. Larlus, V.P. Valchev, Chem. Mater. 16 (2004) 3381.
21. J.P. Verduijn, Eur. Pat. Appl. 0,219,354 (1986).
22. J.P. Verduijn, Int. Pat. WO 91/06367 (1991).
23. J.P. Verduijn, Int. Pat. WO 91/06616 (1991).
24. A.Y. Stakheev, E.S. Shpiro, N.I. Jaeger, G. Schulz-Ekloff, Catal. Lett. 34 (1995) 293.
25. S. Jonpatiwut, P. Sackamduang, T. Rirksomboon, S. Osuwan, W.E. Alvarez, D.E. Resasco, Appl. Catal. A Gen. 230 (2002) 177.
26. M. Tsapatsis, M. Lovallo, T. Okubo, M.E. Davis, M. Sadakata, Chem. Mater. 7 (1995) 1734.
27. D.W.E. Vaughan, K.G. Strohmeier, US Pat.5,318,766 (1994).
28. R.J. Davis, HCR Concise Review, John Wiley and Sons, New York, 1994.
29. R.E. Jentoft, M. Tsapatsis, M.E. Davis, B.C. Gates, J. Catal. 179 (1998) 565.
30. M.A. Camblor, A. Corma, A. Martinez, V. Martinez-Soria, S. Valencia, J. Catal. 179 (1998) 537.
31. S.B. Hong, E. Mielczarski, M.E. Davis, J. Catal. 134 (1992) 349.
32. D.J. Parrillo, A.T. Adamo, G.T. Kokatailo, R.J. Gorte, Appl. Catal. 67 (1990) 107.